Generalized Selective Reduced Integration and {B-bar} Finite Element Methods for Anisotropic Elasticity

Journal:	*International Journal for Numerical Methods in Engineering*
Manuscript ID:	Draft
Wiley - Manuscript type:	Research Article
Date Submitted by the Author:	n/a
Complete List of Authors:	Oberrecht, Stephen; University of California, San Diego, Structural engineering Novak, Jan; Brno University of Technology, Krysl, Petr; University of California, San Diego , Jacobs School of Engineering Department of Structural Engineering
Keywords:	Constitutive equations, Elasticity, Finite element methods, Composites

INTERNATIONAL JOURNAL FOR NUMERICAL METHODS IN ENGINEERING
Int. J. Numer. Meth. Engng 2013; **00**:1–15
Published online in Wiley InterScience (www.interscience.wiley.com). DOI: 10.1002/nme

Generalized Selective Reduced Integration and B-bar Finite Element Methods for Anisotropic Elasticity

S. P. Oberrecht[1], J. Novák[2], P. Krysl[1,*]

[1]*University of California, San Diego, 9500 Gilman Dr., #0085, La Jolla, CA 92093*
[2]*Brno University of Technology, Veveří 331/95, Brno 602 00, Czech Republic*

SUMMARY

Anisotropic elastic materials, such as homogenized model of fiber-reinforced matrix, can display near rigidity under certain applied stress– the resulting strains are small compared to the strains that would occur for other stresses of comparable magnitude. The anisotropic material could be rigid under hydrostatic pressure if the material were incompressible, as in isotropic elasticity, but also for other stresses.
Some commonly used finite element techniques are effective in dealing with incompressibility, but are ill-equipped to handle anisotropic material that lock under stress states that are not mostly hydrostatic (e.g. uniformly reduced serendipity and Q1/Q0 B-bar hexahedra). The failure of the classic B-bar method is attributed to the assumption that the mode of deformation to be relieved is one of near incompressibility. The remedy proposed here is based on the spectral decomposition of the compliance matrix of the material. The spectrum can be interpreted to separate nearly-rigid and flexible modes of stress and strain which leads naturally to a generalized selective reduced integration. Furthermore, the spectral decomposition also enables a three-field elasticity formulation that results in a B-bar method that is effective for general anisotropic materials with an arbitrary nearly-rigid mode of deformation. Copyright © 2013 John Wiley & Sons, Ltd.

Received . . .

KEY WORDS: anisotropic; elasticity; nearly incompressible; rigid stress direction; selective reduced integration; B-bar formulation; finite element;

INTRODUCTION

Selective Reduced Integration (SRI), a method first attributed to the efforts of Doherty et al. [1], has long been considered an effective repair of finite elements that lock under certain modes of deformation. The technique has been given special consideration, for its ability to handle isotropic nearly incompressible elastic solids, where so-called volumetric locking represents a serious difficulty. Hughes [1] describes a formulation based on Lamé parameters, however, an analogous approach based on the split of the deformation energy into terms of bulk and shear moduli yields an alternative [2].

*Correspondence to: University of California, San Diego, 9500 Gilman Dr., #0085, La Jolla, CA 92093

Contract/grant sponsor: Michael Wiese at the Office of Naval Research; contract/grant number: N00014-09-1-0611

A key to the successful implementation of the SRI technique lies in the separation of volumetric and deviatoric energy. As such a split is not clear for solids with anisotropic material responses, traditional SRI is awkward or inapplicable for materials such as fiber-reinforced composites.

This difficulty motivated widespread use of the now familiar B-bar method. In [3], the original B-bar method proposed to treat anisotropic materials, but the separation of volumetric and deviatoric energy as adopted for isotropic materials remained at the heart of this formulation. However, it stands to reason that the nearly-rigid deformation modes can go well beyond the case of vanishing compressibility and the claim that B-bar methods are effective for anisotropic materials has to our knowledge never been tested.

In brief, we separate the mechanical response of anisotropic materials into constrained and unconstrained deformations which are expressed in terms of strain, stress, and energy. Our proposals rest upon the spectral decomposition of the compliance matrix of the material. We rephrase the formulation of Felippa and Oñate [4], and then apply it as an improvement on existing finite element techniques.

The present work is outlined as follows. Section 1 presents a succinct motivation example. In Section 2, the spectral decomposition of the compliance matrix is introduced to separate constrained and unconstrained responses. These results are then used in Section 3 where a discussion of the principal features of the first enhancement technique are given. Since the proposed approach relies on selecting quadrature rules for the generalized split of the material stiffness matrix, it is coined Generalized Selective Reduced Integration (GSRI).

In order to improve the capabilities of the B-bar method as applied to anisotropic elastic solids, in Section 4 we take up a three-field variational elasticity formulation [2] and rephrase it in terms of effective stress and strain. In Section 4, we also strengthen connections to the classical variational formulations revealed by Key [5] and Taylor et al. [6]. Minor modifications to the B-bar technique as developed in Zienkiewicz and Taylor's treatise [2] for isotropic (nearly) incompressible solids are summarized in Section 5, and the resulting corrected B-bar finite element formulation is shown to be an effective remedy for rigidtropic locking in anisotropic solids such as composites with uni-directional reinforcement. Several case studies are provided to assess the ability of the discussed methods to handle materials that are prone to locking in Section 6. Finally, the findings are discussed and conclusions are drawn.

1. MOTIVATION

Consider materials that consist of a soft matrix reinforced with aligned stiff fibers. The system of locally parallel fibers is typically represented macroscopically using material models that have transversely isotropic homogenized properties. We can deduce that for very stiff fibers the material is effectively rigid when loaded in the direction of the fibers. This usually results in underestimated deformations.

By way of motivation, we consider a fiber-reinforced cantilevered beam. The example is discussed in detail in Section 6, but here it suffices to say that the beam is clamped at one end and loaded by a transverse shear force at the free end. The fibers are oriented at an angle with respect to the beam's longitudinal axis given by an orientation vector with components in the Cartesian coordinate system.

Prepared using nmeauth.cls
DOI: 10.1002/nme

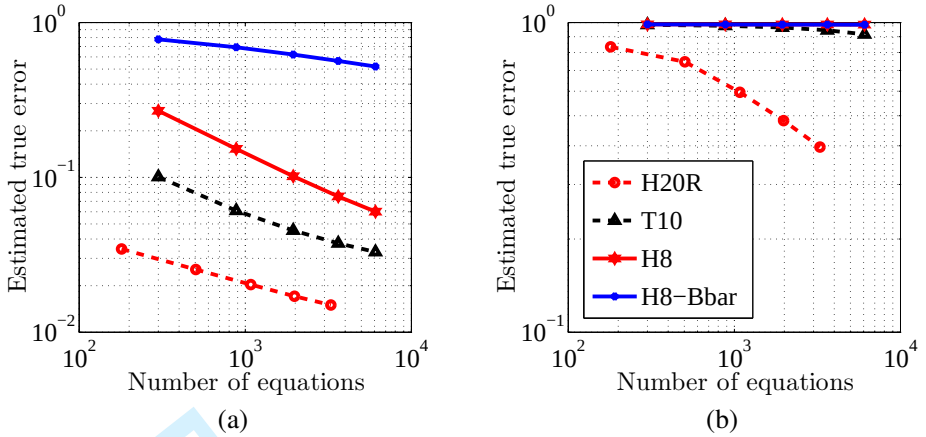

Figure 1. Fiber-reinforced cantilever beam, a) Fiber aligned with $[\sqrt{2}/2, -\sqrt{2}/2, 0]$, b) Fiber aligned with $[\sqrt{2}/2, 0, -\sqrt{2}/2]$. Failure of some common elements to converge satisfactorily (T10 – quadratic tetrahedron. H8 – linear hexahedron, H20 – the uniformly reduced integration quadratic serendipity hexahedron, H8-Bbar – B-bar Q1/Q0 hexahedron as in Hughes [1]).

The x-axis is parallel to the beam's axis, the $z-$axis is vertically transverse. The beam is subject to a distributed shear force at the free end and its structural response, in terms of the normalized true error of the maximum deflection, is shown for a few common finite elements (quadratic tetrahedron T10, linear hexahedron H8, and the uniformly reduced integration quadratic serendipity hexahedron H20 as described in Hughes [1]) in Fig. (1).

It is somewhat surprising that these elements fail to converge satisfactorily. The quadratic tetrahedron does not represent stress well for incompressible elasticity, but at least in displacement converges reasonably well. Not so for this anisotropic model. The serendipity hexahedron normally performs very well for almost incompressible isotropic materials, as has been thoroughly documented [1]. However, it clearly does not properly address locking due to the presence of stiff fibers as demonstrated here. Furthermore, we show that the original B-bar Q1/Q0 formulation [1] leads to no improvement whatsoever with regard to the plain isoparametric hexahedron. Finally, we should note that also the absolute accuracy of all the elements depends strongly upon the orientation of the fiber. For the orientation in Fig. (1)b all the elements are considerably less accurate than for the orientation in Fig. (1)a.

2. SPLIT OF CONSTITUTIVE EQUATION

The idea to use spectral decomposition to represent the strain, stress, and the constitutive relation in linear elasticity goes back a long time. As skillfully reviewed by Helbig [7], these ideas originated with Kelvin's 1856 publication. Another version of this article reappeared in 1878, however not a single citation of this original work can be found until 1984 when Rychlewski [8] formulated an entire theory of constitutive relations based on the spectral decomposition. Quickly thereafter, theoretical publications by Mehrabadi and Cowin [9] and Theocaris [10] followed. These powerful ideas were, to our knowledge, never used in computations.

Here we draw on the recent paper of Felippa and Oñate [4], who make no mention of the prior publications mentioned above. They discuss stress and strain decomposition appropriate to linearly elastic anisotropic materials with volumetric constraints using the spectral decomposition of the compliance matrix. In doing so, they introduce the so-called *rigidtropic* materials, which develop no strains under a stress pattern that follows a null eigenvector of the compliance matrix. Such models include, as a special case, isotropic incompressible materials, for which the eigenvector corresponds to the hydrostatic stress. The main finding contended in [4] is that in anisotropic material models the quantities corresponding to pressure and volumetric strain in incompressible isotropic materials need to be redefined in terms of *effective* quantities [†].

Thus the compliance matrix recast in terms of the spectral decomposition reads

$$\mathbf{D}^{-1} = \frac{1}{3}\sum_{i=1}^{6} \gamma_i \boldsymbol{v}_i \boldsymbol{v}_i^T \ , \tag{1}$$

where γ_i and $\boldsymbol{v}_i$ are the principal value and principal direction of the compliance matrix (eigenvalue and eigenvector), which are assumed to be ordered $\gamma_1 \leq \ldots \leq \gamma_6$, and normalized to length $\sqrt{3}$ through the definition

$$\boldsymbol{v}_j^T \boldsymbol{v}_i = 3\delta_{ji} \ , \tag{2}$$

in order to simplify linkages to isotropic incompressible elasticity. With respect to the decomposition in Eq. (1), a material is called rigidtropic when $\gamma_1 \to 0$ [4]. This means the strain becomes vanishingly small in the direction of $\boldsymbol{v}_1$. To simplify the exposition, we will consider the case of a single principal compliance approaching zero at first and focus on a material with two or more rigidtropic modes in the sequel to this work.

Using the above decomposition, the compliance matrix may be split into the constrained (rigid) and the unconstrained (flexible) parts, respectively, as

$$\mathbf{D}^{-1} = \frac{1}{3}\gamma_1 \boldsymbol{v}_1 \boldsymbol{v}_1^T + \frac{1}{3}\sum_{i=2}^{6} \gamma_i \boldsymbol{v}_i \boldsymbol{v}_i^T \ . \tag{3}$$

It may be shown, as in Reference [4], that for isotropic incompressible materials

$$\boldsymbol{v}_1 = [1,1,1,0,0,0]^T,$$

and we obtain as the constrained/unconstrained split the volumetric/deviatoric partitioning of the constitutive equation.

[†]A material is called "effectively" rigid when it undergoes zero strains under a stress pattern proportional to the eigenvector associated with a zero principal compliance. Here, the term "effective" has no relation to its meaning in homogenization theory.

Prepared using nmeauth.cls
DOI: 10.1002/nme

3. GENERALIZED SELECTIVE REDUCED INTEGRATION

The SRI scheme is a venerable technique for treatment of isotropic incompressible materials with standard finite elements (see [3, 1] for relevant background). In this section we briefly introduce a generalization that facilitates the method's handling of constrained anisotropic media.

Consider, as a starting point, the total potential energy of an infinitesimal deformable elastic body in the form

$$\mathcal{U} = \frac{1}{2}\boldsymbol{\epsilon}^T \mathbf{D} \boldsymbol{\epsilon} \,, \tag{4}$$

where $\boldsymbol{\epsilon} = [\epsilon_{11}, \epsilon_{22}, \epsilon_{33}, 2\epsilon_{32}, 2\epsilon_{31}, 2\epsilon_{12}]^T$ is the Voigt-Mandel representation of the second order strain tensor and the material stiffness matrix $\mathbf{D}$ follows from Eq. (1) as

$$\mathbf{D} = \sum_{i=1}^{6} \frac{1}{3\gamma_i} \boldsymbol{v}_i \boldsymbol{v}_i^T \,. \tag{5}$$

The quantity

$$K_i = \frac{1}{3\gamma_i} \,, \tag{6}$$

is referred to as the effective stiffness (designated the "effective bulk modulus" in Reference [4]).

By analogy to Eq. (1), the material stiffness can be recast as

$$\mathbf{D} = \mathbf{D}_r + \mathbf{D}_f \,, \tag{7}$$

where for the rigid and flexible contributions, respectively, we have

$$\mathbf{D}_r = K_1 \boldsymbol{v}_1 \boldsymbol{v}_1^T, \quad \mathbf{D}_f = \sum_{i=2}^{6} K_i \boldsymbol{v}_i \boldsymbol{v}_i^T \,. \tag{8}$$

Substituting Eq. (7) into Eq. (4) leads to what can be viewed as an additive split of the constrained and unconstrained energy contributions. Applying carefully chosen integration rules to each of these energies–full integration to the flexible part and reduced integration to its nearly rigid counter part– leads to the GSRI technique. A variant of the B-bar formulation will be presented as an alternative to the GSRI method in Section 5.

4. THREE-FIELD FORMULATION OF ANISOTROPIC ELASTICITY

Introducing two simple relations, to be used in a mixed approximation, provides a novel treatment for rigidtropic materials. First define the effective constrained stress as

$$p = \frac{1}{3}\boldsymbol{m}^T \boldsymbol{\sigma} \,, \tag{9}$$

and the effective constrained strain in the form

$$\epsilon_v = \boldsymbol{m}^T \boldsymbol{\epsilon} \,. \tag{10}$$

DOI: 10.1002/nme

Here, the strain field is derived from the displacement vector as $\boldsymbol{\epsilon} = \mathbf{B}\boldsymbol{u}$. For a clear backward compatibility with isotropic nearly incompressible elasticity we keep the notation p (i.e. pressure) and ϵ_v (i.e. volumetric strain). For isotropic materials the vector $\boldsymbol{m}$ reads as

$$\boldsymbol{m} = [1, 1, 1, 0, 0, 0]^T \,. \tag{11}$$

In this study, we take

$$\boldsymbol{m} = \boldsymbol{v}_1 \,, \tag{12}$$

which allows to write the constitutive relation between the effective pressure and the volumetric strain in the form

$$p = K_1 \epsilon_v \,. \tag{13}$$

Next, the unconstrained stress (i.e. the deviatoric stress in isotropic elasticity) is linked to the unconstrained strain as

$$\boldsymbol{\sigma}_d = \mathbf{D}_d \boldsymbol{\epsilon} \,, \tag{14}$$

where we use $\mathbf{D}_d = \mathbf{D}_f$. Again, for backward compatibility we use the notation $\mathbf{D}_d$, which for isotropic materials refers to the deviatoric part of the material stiffness matrix. The total stress then becomes

$$\boldsymbol{\sigma} = \boldsymbol{\sigma}_d + p\boldsymbol{m} \,.$$

Therefore, the principle of virtual work is rendered as

$$\int_\Omega \delta\boldsymbol{\epsilon}^T \left(\boldsymbol{\sigma}_d + p\boldsymbol{m}\right) \,\mathrm{d}\Omega - \int_\Omega \delta\boldsymbol{u}^T \boldsymbol{b} \,\mathrm{d}\Omega - \int_{\Gamma_t} \delta\boldsymbol{u}^T \boldsymbol{t} \,\mathrm{d}\Gamma = 0 \,, \tag{15}$$

or, introducing Eq. (14),

$$\int_\Omega \delta\boldsymbol{\epsilon}^T \mathbf{D}_d \mathbf{B}\boldsymbol{u} \,\mathrm{d}\Omega + \int_\Omega \delta\boldsymbol{\epsilon}^T p\boldsymbol{m} \,\mathrm{d}\Omega - \int_\Omega \delta\boldsymbol{u}^T \boldsymbol{b} \,\mathrm{d}\Omega - \int_{\Gamma_t} \delta\boldsymbol{u}^T \boldsymbol{t} \,\mathrm{d}\Gamma = 0 \,. \tag{16}$$

Note, that in the above equlibrium/static relations the vector $\boldsymbol{b}$ stands for the generalized forces in a body Ω, and $\boldsymbol{t}$ represents the Neumann boundary conditions on the traction boundary Γ_t. Next, Eq. (16) is supplemented with the weakly enforced kinematics in Eq. (10)

$$\int_\Omega \delta p \left(\boldsymbol{m}^T \mathbf{B}\boldsymbol{u} - \epsilon_v\right) \,\mathrm{d}\Omega = 0 \,, \tag{17}$$

where $\mathbf{B}$ is the standard symmetric gradient operator [2] and with the weak form of the constitutive equation (13)

$$\int_\Omega \delta\epsilon_v \left(K_1 \epsilon_v - p\right) \,\mathrm{d}\Omega = 0 \,. \tag{18}$$

Equations (16), (17) and (18) constitute together with Eq. (12), the three-field $\boldsymbol{u} - p - \epsilon_v$ formulation of *anisotropic* elasticity. For isotropic elastic materials the above formulation is identical to that described in the literature, see e.g. [2].

Similar variational formulation was developed by Key [5]. Key considers incompressible materials and develops a modified Reissner-Hellinger principle that includes pressure as an

independent variable. The possibility of replacing pressure with "extensional stress variable" is also mentioned in passing.

Furthermore, Taylor et al. [6] have developed a formulation based on additional pressure and dilatation variables. The projection vector defined in equation (11) of the treatise [6] denotes the direction of hydrostatic stress, which the authors observe to be appropriate for both isotropic and anisotropic elastic materials with (nearly) zero dilatation.

As this choice is the same one made in the original formulation of the B-bar technique [3], it is largely ineffective in dealing with fiber-reinforced materials where the rigidity constraints are other than volumetric. As such, it is not suited to deal with specific anisotropic materials whose rigidity differs from the condition of near incompressiblity.

5. B-BAR VARIANT FORMULATION

To treat Eqs. (16, 17) and (18) with the finite element method the following approximations are adopted (we use the notation of [2])

$$\boldsymbol{u} \approx \mathbf{N}_u \tilde{\boldsymbol{u}}, \quad p \approx \mathbf{N}_p \tilde{\boldsymbol{p}}, \quad \epsilon_v \approx \mathbf{N}_v \tilde{\boldsymbol{\epsilon}}_v \,. \tag{19}$$

Moreover, it is assumed that $\mathbf{N}_v$ equals $\mathbf{N}_p$, for reasons discussed in [2]. We also appeal to the "discontinuous pressure/condensation" formulation so that the p and ϵ_v variables can be eliminated locally on the element basis. The mixed approximation is thus obtained in the form

$$\begin{bmatrix} \mathbf{A} & \mathbf{C} & \mathbf{0} \\ \mathbf{C}^T & \mathbf{0} & -\mathbf{E} \\ \mathbf{0} & -\mathbf{E}^T & \mathbf{H} \end{bmatrix} \begin{Bmatrix} \tilde{\boldsymbol{u}} \\ \tilde{\boldsymbol{p}} \\ \tilde{\boldsymbol{\epsilon}}_v \end{Bmatrix} = \begin{Bmatrix} \boldsymbol{f}_1 \\ \mathbf{0} \\ \mathbf{0} \end{Bmatrix} . \tag{20}$$

The matrices above are defined as [2]

$$\mathbf{I}_d = \mathbf{I} - \frac{1}{3}\boldsymbol{m}\boldsymbol{m}^T, \quad \mathbf{A} = \int_\Omega \mathbf{B}^T \mathbf{D}_d \mathbf{B} \, \mathrm{d}\Omega, \quad \mathbf{E} = \int_\Omega \mathbf{N}_v^T \mathbf{N}_p \, \mathrm{d}\Omega,$$
$$\mathbf{H} = \int_\Omega \mathbf{N}_v^T K_1 \mathbf{N}_v \, \mathrm{d}\Omega, \quad \mathbf{C} = \int_\Omega \mathbf{B}^T \boldsymbol{m} \mathbf{N}_p \, \mathrm{d}\Omega \,. \tag{21}$$

Eliminating the effective strain from the second equation yields

$$\tilde{\boldsymbol{\epsilon}}_v = \mathbf{E}^{-1}\mathbf{C}^T \tilde{\boldsymbol{u}} = \mathbf{W}\tilde{\boldsymbol{u}} \,, \tag{22}$$

where we introduce $\mathbf{W} = \mathbf{E}^{-1}\mathbf{C}^T$, so that substitution into the third term in Eq. (20) gives

$$\tilde{\boldsymbol{p}} = \mathbf{E}^{-T}\mathbf{H}\tilde{\boldsymbol{\epsilon}}_v = \mathbf{E}^{-T}\mathbf{H}\mathbf{W}\tilde{\boldsymbol{u}} \,. \tag{23}$$

Finally we obtain the linear system in terms of the displacements only

$$\bar{\mathbf{A}}\tilde{\boldsymbol{u}} = \boldsymbol{f}_1 \,, \tag{24}$$

Prepared using nmeauth.cls
DOI: 10.1002/nme

where

$$\bar{\mathbf{A}} = \mathbf{A} + \mathbf{W}^T \mathbf{H} \mathbf{W} \,, \tag{25}$$

by making use of the first row in Eq. (20). It follows from Eq. (16), Eq. (18) and approximations in Eq. (19), that we can write Eq. (26) as

$$\bar{\mathbf{A}} = \int_\Omega \mathbf{B}^T \mathbf{D}_d \mathbf{B} \, \mathrm{d}\Omega + \int_\Omega \mathbf{W}^T \mathbf{N}_v^T K_1 \mathbf{N}_v \mathbf{W} \, \mathrm{d}\Omega \,. \tag{26}$$

Noting the relations for the effective stiffness

$$\mathbf{D}_d = \mathbf{I}_d \mathbf{D} \mathbf{I}_d \,, \quad K_1 = \frac{1}{3} \boldsymbol{m}^T \mathbf{D} \frac{1}{3} \boldsymbol{m} \,, \tag{27}$$

allows recasting Eq. (26) as

$$\bar{\mathbf{A}} = \int_\Omega \mathbf{B}^T \mathbf{I}_d \mathbf{D} \mathbf{I}_d \mathbf{B} \, \mathrm{d}\Omega + \int_\Omega \mathbf{W}^T \frac{1}{3} \mathbf{N}_v^T \boldsymbol{m}^T \mathbf{D} \frac{1}{3} \boldsymbol{m} \mathbf{N}_v \mathbf{W} \, \mathrm{d}\Omega \,. \tag{28}$$

Finally, Eq. (28) combines to form

$$\int_\Omega \left[\left(\mathbf{I}_d \mathbf{B} + \frac{1}{3} \boldsymbol{m} \mathbf{N}_v \mathbf{W} \right)^T \mathbf{D} \left(\mathbf{I}_d \mathbf{B} + \frac{1}{3} \boldsymbol{m} \mathbf{N}_v \mathbf{W} \right) \right] \mathrm{d}\Omega = \int_\Omega \bar{\mathbf{B}}^T \mathbf{D} \bar{\mathbf{B}} \, \mathrm{d}\Omega \,, \tag{29}$$

where the assumed-strain B-bar matrix reads

$$\bar{\mathbf{B}} = \mathbf{I}_d \mathbf{B} + \frac{1}{3} \boldsymbol{m} \mathbf{N}_v \mathbf{W} \,. \tag{30}$$

Note that the $\mathbf{W}$ matrix is calculated from the three-field coupling terms $\mathbf{E}$ and $\mathbf{C}$, which could be integrated with a different, lower, quadrature rule than that used for the remaining portion of the element stiffness matrix (29). We have discovered no cases where there is an advantage to be gained by integrating the constituents of the $\mathbf{W}$ matrix with the same quadrature rule as that employed for the stiffness matrix itself. Therefore we use a reduced rule for this purpose. The computed maximum displacements and strain energies for runs with the fully integrated and reduced-order integrated $\mathbf{W}$ matrix agree with one another to several decimal places for all of the examples investigated. The two methods, the GSRI and the B-bar method, consequently use a pair of Gauss quadrature rules each: the integration rule pairs are denoted (1,2) for the linear elements and (2,3) for the quadratic elements. The first number of the rule indicates the number of Gauss points per dimension for the stiffness matrix corresponding to the nearly-rigid modes of deformation (GSRI) or the $\mathbf{W}$ matrix (B-bar), and the second number indicates the number of Gauss points per dimension stiffness matrix corresponding to the flexible modes of deformation (GSRI) or the stiffness matrix (B-bar).

Note that the discrete formulation in this section exactly mirrors that of Reference [2]. The only difference is the use of *effective strain, stress, and moduli* stemming from the spectral decomposition of the compliance (or stiffness) matrix of the material. For isotropic materials the present formulation is identical to that based on the volumetric/deviatoric split.

DOI: 10.1002/nme

6. EXAMPLES

We introduce three examples based on simple cantilevered structures. The rigidtropic materials have a single dominant fiber direction that can be applied at any angle determined by local coordinate rotations. The chosen loading results in significant locking behavior for all elements that are not treated by use of the spectral decomposition of the anisotropic elastic constitutive relation. Although this behavior can be verified with similar results in other elements, such as tetrahedra, we focus our attention on linear and quadratic hexahedral "brick" elements.

Each example is one of two geometric configurations with similar boundary conditions: a slender cantilevered beam or a cantilevered plate. The beam's dimensions are: $W = 6.5\ \text{cm}$, $L = 5.81\ \text{cm}$, and $t = 1.29\ \text{cm}$. Here L is the length, W is the width, and t is the thickness. The plate's dimensions are the same except $W = 6.45\ \text{cm}$.

The domain Ω of sought finite element solutions are given by $x \in [0, L]$, $y \in [0, W]$, and $z \in [0, t]$. The Dirichlet boundary conditions on Γ_u at $x = 0$, Fig. (2)a, are

$$u_x = u_y = u_z = 0\,. \tag{31}$$

The Neumann boundary conditions are prescribed on Γ_t at $x = L$ as

$$\sigma \cdot \hat{n} = \tau_{xz} = -689\ \text{kPa}. \tag{32}$$

Note that $\Gamma = \Gamma_t \cup \Gamma_u$ and $\Gamma_t \cap \Gamma_u = \varnothing$. The boundary conditions remain the same throughout the examples.

The convergence of the treated elements is demonstrated for each example and calculated errors are referenced with respect to the limit of the quadratic refinement for the respective models, as determined by Richardson's extrapolation [11]. The refinement was carried out with a progressively increasing Number of Degrees-Of-Freedom ($NDOF$). For the linear, eight node, hexahedral elements (H8) $NDOF = [216,\ 1134,\ 3240,\ 7020,\ 12960,\ 21546,\ 33264,\ 48600]$, and for quadratic, 27 node, hexahedral elements (H27) $NDOF = [1134,\ 7020,\ 21546,\ 48600]$. The strain energy errors are reported graphically and are defined by the error expression as

$$\Psi = \frac{\mathcal{U}}{\mathcal{U}_\xi} - 1\,, \tag{33}$$

where Ψ is the error, $\mathcal{U}$ is the computed strain energy, and $\mathcal{U}_\xi$ is the limit value arising from Richardson's extrapolation.

In these examples, the maximum deflection at the free ends of the beam and plate, as well as the strain energy error, are plotted with four different element treatments. The first two, in subsequent figures denoted as "GSRI*" and "B-bar*," ignore the principal compliance and take the rigid component to be constructed by means of $\boldsymbol{m} = [1, 1, 1, 0, 0, 0]^T$. This blindly treats the anisotropic material as one might with simple selective reduced integration tailored for volumetric locking in nearly incompressible isotropic materials. By contrast, this demonstrates the effectiveness of "unlocking" the rigid modes through the proposed spectral decomposition.

The second, suggested, two treatments are denoted "GSRI" and "B-bar", and they use the principal compliance's first mode $\boldsymbol{v}_1$ to identify the nearly rigid component.

DOI: 10.1002/nme

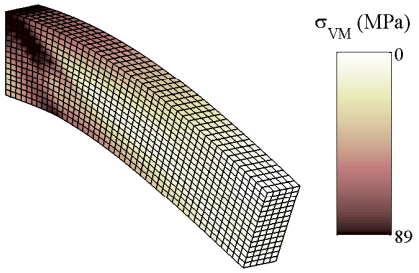

Figure 2. The linear hexahedral element with the corrected B-bar formulation: deflection with 12960 degrees-of-freedom is shown. Displacement values are scaled up by a factor of 50 and the von-Mises stresses are viewed as a color-field. The maximum displacement realized at the free end is $\mathrm{u}_{\max} = 0.329\ \mathrm{mm}$.

The first example was described as a motivation of this paper and is reviewed here in greater detail. In Figs. (2–4) we demonstrate the results for a simple beam model with a stiff fiber reinforcement along the vector $[\sqrt{2}/2, 0, -\sqrt{2}/2]$ (compare with Figure 1b).

The elastic modulus along the stiff fiber is 20,000 times higher than in the transverse directions, and the shear terms comparatively very small in magnitude. The anisotropic elastic properties are

$E_1 = 137895\ \mathrm{GPa}, \quad E_2 = E_3 = 6.895\ \mathrm{GPa}, \quad G_{12} = G_{13} = 3.45\ \mathrm{GPa}, \quad G_{23} = 1.38\ \mathrm{GPa}, \quad$ and $\nu_{12} = \nu_{13} = \nu_{23} = 0.25$.

The spectral decomposition reveals that as the ridigity of the fibers increase without bound, the nearly-zero strains are directed along

$$\boldsymbol{v}_1 = \sqrt{3}[1, 0, 0, 0, 0, 0]^T \tag{34}$$

in the local (fiber-aligned) coordinates. Figure 2 shows the deformed shape color-coded with von Mises stress for the corrected B-bar formulation with linear hexahedra. The effect of the reinforcing fibers that leads to a strong variation of the stress along the fibers anchored in the clamped face is clearly visible. Figure 3 clearly illustrates that satisfactory convergence in energy can not be expected from finite elements that use the ineffective formulation for the isotropic nearly-incompressible materials (i.e. the standard B-bar technique); the corrected GSRI and B-bar formulations deliver identical solutions that converge well. Figure 4 shows the convergence in energy for the quadratic hexahedron. While the elements converge better than the linear ones for the incorrect formulation, the corrected techniques are clearly superior.

Next, in Figs. (5–7) we illustrate the performance for a cantilevered plate reinforced with stiff fibers oriented in parallel alignment with the arbitrarily chosen unit vector $\boldsymbol{n} = [0.933012701892219, 0.258819045102521, -0.250000000000000]^T$. The anisotropic material properties are as in the previous example.

In Figure 5 we show the deflected shape of the fiber-reinforced cantilevered plate. The von-Mises stress is again indicated by color. Figure 6 illustrates the slow convergence of the elements without the improvement, and the robust performance of the corrected method. Figure 7 shows again that

DOI: 10.1002/nme

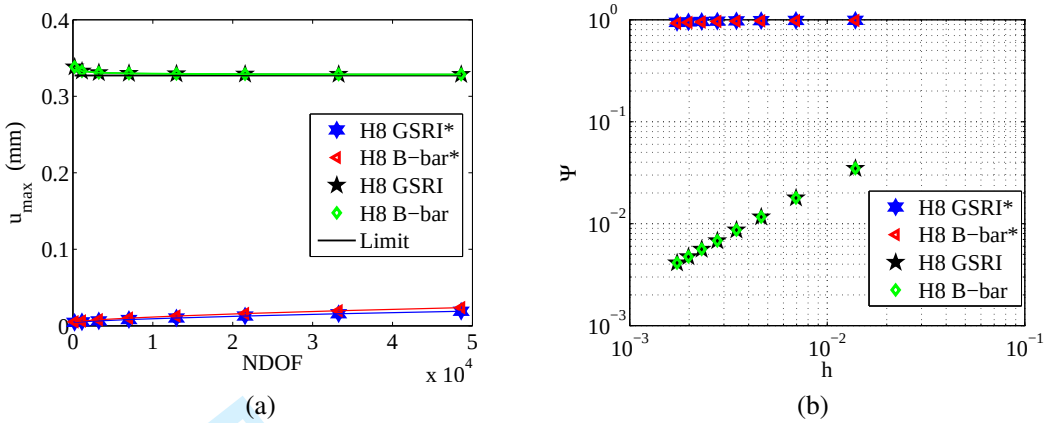

Figure 3. For the fiber-reinforced cantilevered beam, untreated H8 elements fail to converge satisfactorily. a) The maximum displacement at free end versus discretization density. b) The strain energy error versus discretization density.

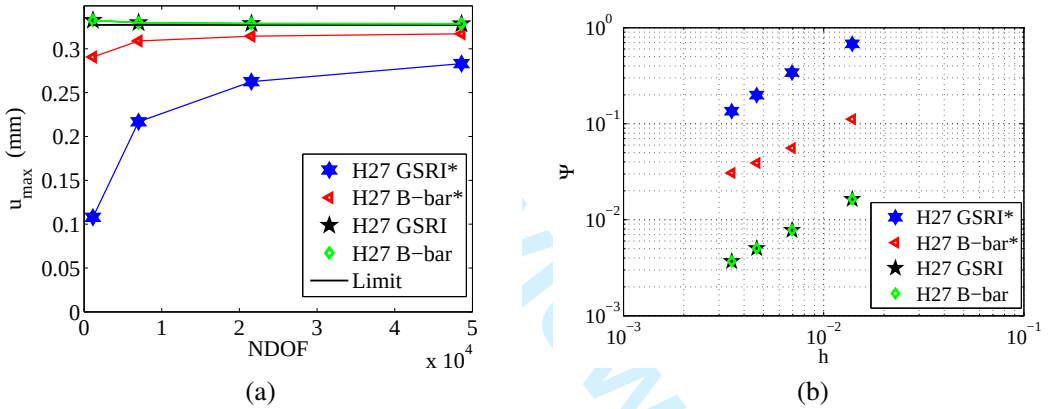

Figure 4. For the single-fiber cantilevered beam with H27 elements, the treated elements show improved convergence. a) The maximum displacement at free end versus discretization density, converge to $u_{max} = 0.3272$ mm. b) The strain energy error versus discretization density.

the convergence can be improved by using a higher-order element, but without the correction the convergence will not be satisfactory.

Finally, we demonstrate with Figs. (8–10), the performance capabilities when the mesh is subjected to significant distortion. The solutions with the distorted meshes match the maximum displacement and strain energy values of the well-proportioned uniform meshes, showing that the treatments remain robust even when the discretization is far from ideal. The maximum deflection of the plate converges to $u_{max} = 0.085291$ mm with a uniform mesh and to $u_{max} = 0.085197$ mm with a distorted mesh.

The spectral analyses of single element stiffness matrices for three different element treatments are compared in Fig. (11) For both linear and quadratic hexahedra (H8 and H27 respectively) we compare the GSRI formulation with B-bar formulations for different quadrature rules. We use either the quadrature rule pairs (1,2) for the linear elements and (2,3) for the quadratic elements (the "reduced" rules), or the quadrature rule pairs (2,2) for the linear elements and (3,3) for the quadratic elements (the "full" rules). The full-quadrature B-bar treatment is labeled "B-bar[1]," and

Prepared using nmeauth.cls
DOI: 10.1002/nme

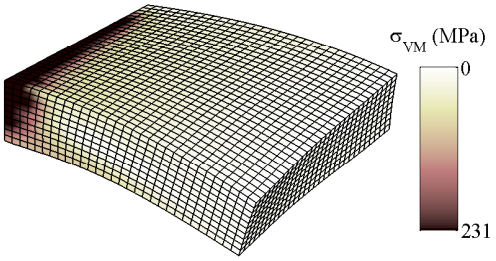

Figure 5. The linear hexahedral element B-bar solution of a fiber-reinforced cantilevered plate with 30690 degrees-of-freedom is shown. Displacement values are scaled up by a factor of 200 and the von-Mises stresses are viewed as a color-field. The maximum displacement at the free end is $u_{max} = 0.0901$ mm.

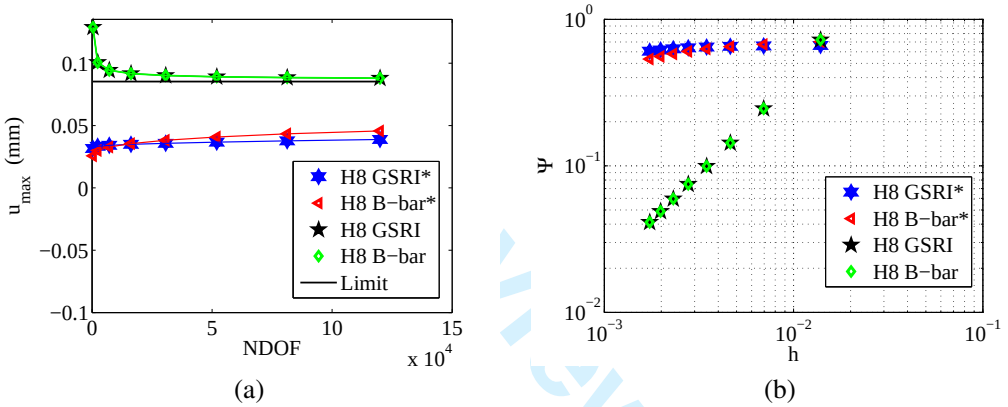

Figure 6. For the fiber-reinforced cantilevered plate, untreated H8 elements fail to converge satisfactorily. a) The maximum displacement at free end versus discretization density. b) The strain energy error versus discretization density.

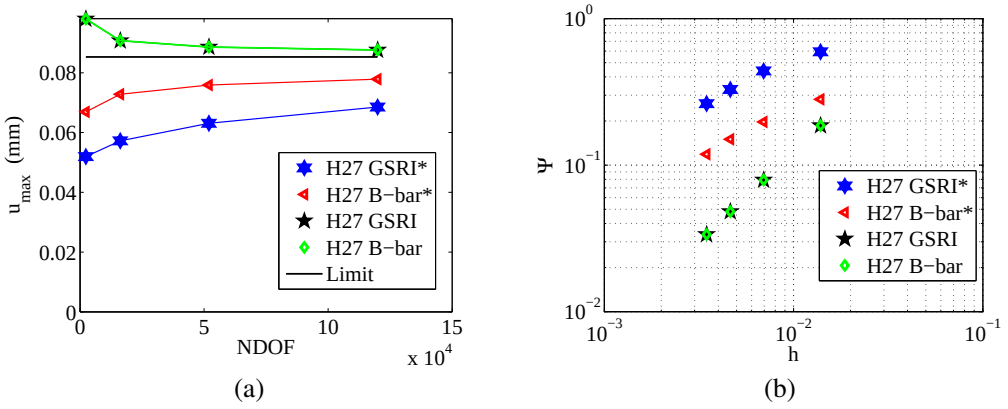

Figure 7. For the single-fiber cantilevered plate with H27 elements, the treated elements show improved convergence. a) The maximum displacement at free end versus discretization density. b) The strain energy error versus discretization density.

DOI: 10.1002/nme

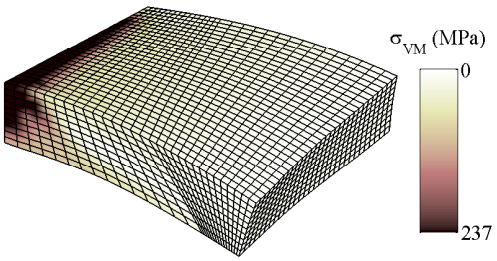

Figure 8. The linear hexahedral element B-bar solution of a fiber-reinforced cantilevered plate with a severely distorted mesh. The model with 30690 degrees-of-freedom is shown. Displacement values are scaled up by a factor of 200 and the von-Mises stresses are viewed as a color-field. The maximum displacement realized at the free end is $u_{max} = 0.0886$ mm.

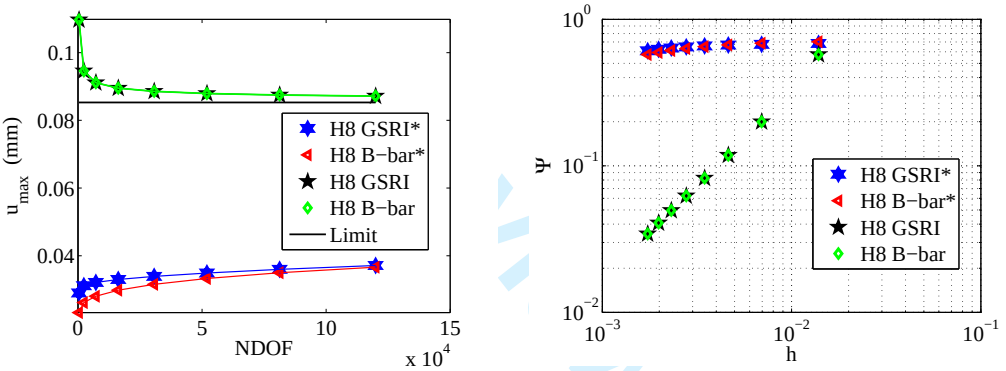

Figure 9. For the fiber-reinforced cantilevered plate with mesh distortion, untreated H8 elements fail to converge satisfactorily. a) The maximum displacement at free end versus discretization density. b) The strain energy error versus discretization density..

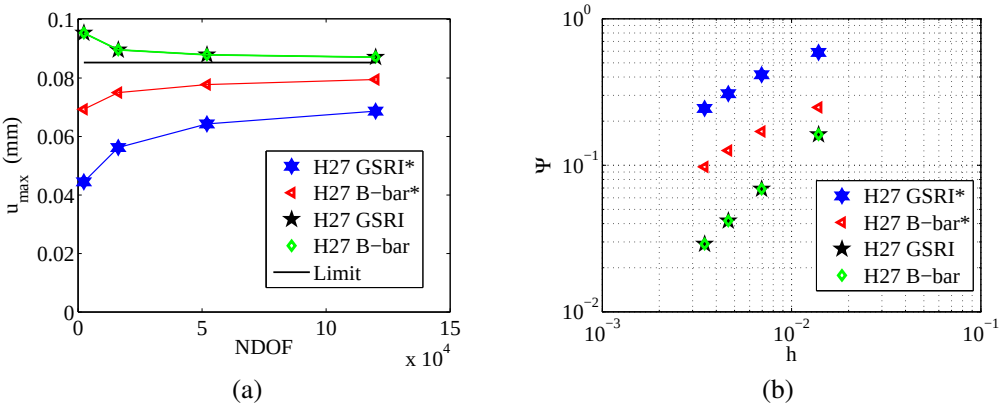

Figure 10. For the distorted single-fiber cantilevered plate with H27 elements, the treated elements show improved convergence. a) The maximum displacement at free end versus discretization density. b) The strain energy error versus discretization density.

Prepared using nmeauth.cls
DOI: 10.1002/nme

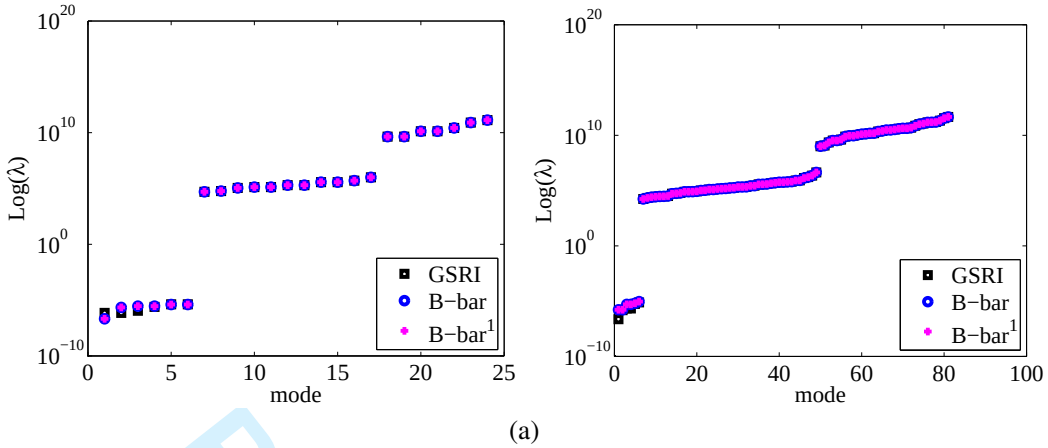

Figure 11. The spectral analysis of the a single element stiffness matrix including the six rigid body modes. a) The eigenvalues for proposed linear hexahedra. b) The eigenvalues for proposed quadratic hexahedra.

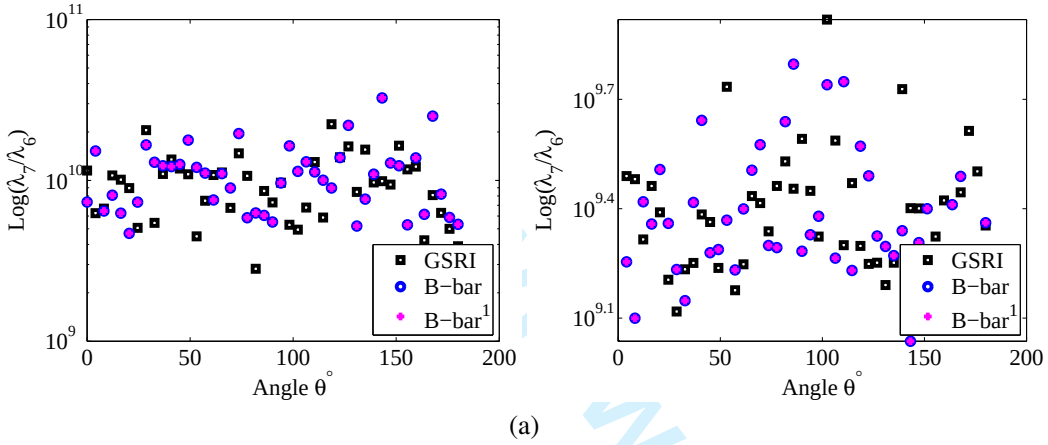

Figure 12. The ratio of the seventh to sixth eigenvalues for a single element stiffness matrix is an indicator of stability; values much greater than one indicate element stability. a) The ratio λ_7/λ_6 for treated H8 elements. b) The ratio λ_7/λ_6 for treated H27 elements.

it is included to show that using the reduced-rule the B-bar variant does not affect the resulting stability of the elements.

The ranks of the H8 elements and H27 elements show a deficiency of six, one for each rigid body mode. Moreover, it can be seen in Fig. (12) that the eigenvalues of the 7th mode are several orders of magnitude greater than the first six, which are numerically equivalent to zero eigenvalues for the respective element stiffness matrices. This demonstrates that the proposed elements have a full rank with either the reduced rule or with the full rule and are therefore stable.

CONCLUSIONS

The treatments of anisotropic elasticity with nearly-rigid locking through a partitioning of the strain, stress, and the constitutive equation by both generalized selective reduced integration (GSRI) and the corrected B-bar formulations are found to be robust and effective. The performance of the

DOI: 10.1002/nme

two proposed methods are nearly identical. The corrected B-bar method is moreover attractive due to its generality for potential application to nonlinear materials. The correction is inexpensive: the treated methods do not require any special computations except for the spectral decomposition of the compliance matrix. As such, a computation is only required once for each material (in the material-aligned coordinate system); such a cost is likely to be negligible.

Extension of the proposed techniques to treatment of materials with multiple nearly-rigid deformation modes is currently under investigation.

ACKNOWLEDGEMENTS

The work of Jan Novák was sponsored by the European Social Fund under Grant No. CZ.1.07/2.3.00/30.0005 (Support for the creation of excellent interdisciplinary research teams at Brno University of Technology) and GAČR 13-22230S.

REFERENCES

1. Hughes TJR. *The Finite Element Method - Linear Static and Dynamic Finite Element Analysis*. Dover Publications, Inc., 2000.
2. Zienkiewicz O, Taylor R. *The Finite Element Method: The Basis*. Oxford [etc.] : Butterworth Heinemann, 2000.
3. Hughes TJR. Generalization of selective integration procedures to anisotropic and non-linear media. *International Journal for Numerical Methods in Engineering* 1980; **15**(9):1413–1418.
4. Felippa CA, Onate E. Stress, strain and energy splittings for anisotropic elastic solids under volumetric constraints. *Computers & Structures* 2003; **81**(13):1343–1357.
5. Key SW. A variational principle for incompressible and nearly-incompressible anisotropic elasticity. *International Journal of Solids and Structures* 1969; **5**(9):951–964.
6. Taylor RL, Pister KS, Herrmann LR. On a variational theorem for incompressible and nearly-incompressible orthotropic elasticity. *International Journal of Solids and Structures* 1968; **4**(9):875–883.
7. Helbig K. Review paper: What Kelvin might have written about Elasticity. *Geophysical Prospecting* 2013; **61**(1):1–20.
8. Rychlewski J. On Hooke law. *Pmm Journal of Applied Mathematics and Mechanics* 1984; **48**(3):303–314.
9. Mehrabadi MM, Cowin SC. Eigentensors of linear anisotropic elastic-materials. *Quarterly Journal of Mechanics and Applied Mathematics* 1990; **43**:15–41.
10. Theocaris PS, Philippidis TP. Spectral decomposition of compliance and stiffness 4th-rank tensors suitable for orthotropic materials. *Zeitschrift Fur Angewandte Mathematik Und Mechanik* 1991; **71**(3):161–171.
11. Krysl P. *Thermal and Stress Analysis with the Finite Element Method*. Pressure Cooker Press: San Diego, 2013.

DOI: 10.1002/nme